ACS SENSORS

pubs.acs.org/acssensors Article

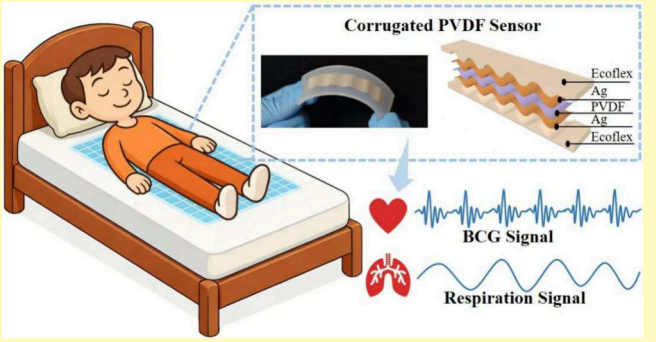
A Corrugated PVDF-Based Flexible Piezoelectric Sensor for Physiological Signal Detection

Ziqiong Cao, Donglin Wu, Yaojun Yuan, Rui Hu, Jiaqi Zhang, Enting Gao, Xinjian Chen, Xuemei Lu, Xiaoyu Tang, and Baoqing Nie*

Cite This: *ACS Sens.* 2026, 11, 2731−2740 Read Online

ACCESS | Metrics & More | Article Recommendations | Supporting Information

ABSTRACT: Continuous monitoring of heart rate and respiration is vital for disease diagnosis and health management. Flexible polyvinylidene fluoride (PVDF) piezoelectric sensors can accurately acquire these signals, thereby providing critical data support for health management. Current high-performance PVDF sensors typically enhance properties by doping functional materials but suffer from complex fabrication procedures and difficulties in composition control. In this study, we propose a flexible piezoelectric sensor based on a corrugated polyvinylidene fluoride (PVDF) film for contactless physiological signal monitoring. By using a simple template molding method, the corrugated PVDF film (CPF) is shaped into a uniform wavy configuration and encapsulated in a soft elastomer to preserve its geometry. The wave design enhances the spatial freedom of PVDF deformation, and the elastic encapsulation layer facilitates rapid shape recovery. The two effects synergistically improve the piezoelectric output and dynamic response of the sensor. The CPF-based sensor exhibits a sensitivity of 0.36 V/N, a minimum detectable force of 98 mg, and a fast response/recovery time of less than 0.1 ms. By integrating with a soft cushion, the sensor is capable of detecting subtle vibrations caused by thoracic and cardiac movements once people lie or sit on the smart cushion. Moreover, it reliably captures pulse waveforms at multiple body locations, demonstrating its promising potential for noncontact physiological signal monitoring.

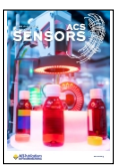


KEYWORDS: *piezoelectric sensor, corrugated PVDF, ballistocardiography (BCG), respiratory monitoring, smart cushion*

Human physiological signals such as the heart rate, blood pressure, respiration rate, body temperature, and pulse wave are essential parameters for evaluating an individual's health status and physiological conditions.[1−4] Continuous monitoring of the heart rate and respiration is particularly important for disease diagnosis and health management.[5,6] Electrocardiography (ECG) and thoracic impedance are commonly used techniques for measuring these signals induced by heart activities.[7,8] However, both methods typically require direct skin contact and may cause discomfort during long-term monitoring, especially for elderly individuals or infants. Photoplethysmography (PPG) offers another noninvasive and comfortable solution for multiple physiological signal detections, while it is susceptible to interference from ambient light and pressure.[9] Instead, ballistocardiography (BCG)-based health monitoring systems offer a continuous, comfortable, and reliable alternative.[10,11]BCG captures microvibrations generated by cardiac contractions and blood flow, enabling contactless signal acquisition. Various sensing techno- logies have been employed to capture BCG signals, including pressure sensors,[10−12] accelerometers,[13,14] optical sensors,[15,16] radar sensors,[17,18] and piezoelectric sensors.[19,20] Pressure sensors and accelerometers are low-cost and easily integrable, yet they are susceptible to motion artifacts and environmental interferences. Radar sensors provide high accuracy and penetration capability but come with higher cost and system complexity.[21] Optical sensors offer high sensitivity but require stringent environmental conditions and are vulnerable to light interference.[22]

Among contactless BCG signal monitoring technologies, piezoelectric sensors have attracted significant attention due to their high sensitivity, low power consumption, and rapid response.[23,24] Although traditional piezoelectric ceramics exhibit high sensitivity, their rigidity limits their suitability for direct contact with the human body.[25] Flexible piezoelectric materials, such as polyvinylidene fluoride (PVDF) and its copolymers, have been widely employed in physiological monitoring systems, owing to their lightweight nature, softness, excellent fatigue resistance, and biocompatibility.[26,27] Current research focuses on enhancing the piezoelectric performance of PVDF-based materials by optimizing

Received: July 25, 2025
Revised: January 19, 2026
Accepted: January 20, 2026
Published: February 3, 2026



ACS Publications © 2026 American Chemical Society

https://doi.org/10.1021/acssensors.5c04749
ACS Sens. 2026, 11, 2731−2740

Downloaded from pubs.acs.org/acscfj/article-pdf/11/3/2731/6490049/se-2025-04749j.pdf by SOOCHOW UNIV user on 13 October 2026

their intrinsic properties[28−31] and developing advanced sensing structures.[32−34] However, those methods often involve complex synthesis procedures, fabrication processes, or difficulties in composition control.

In this study, we design a flexible piezoelectric force/pressure sensor based on a corrugated PVDF film (CPF) for physiological signal detections. The PVDF film, coated with silver electrodes on both surfaces, is shaped into a uniform wavy structure using a simple customized mold and encapsulated with platinum-catalyzed silicone rubber (Ecoflex). The corrugated configuration enhances the freedom of PVDF deformation and improves its responsiveness to external stimuli. Additionally, the elastic encapsulation material promotes rapid shape recovery of the PVDF layer, significantly enhancing the dynamic characteristics of the sensor. Compared to flat-structured sensors, the corrugated design demonstrates a high sensitivity of 0.36 V/N, with a 2.77-fold increment. The CPF-based piezoelectric sensor exhibits a minimum resolution of 98 mg and fast response and recovery times of less than 0.1 ms. By integrating into a soft cushion, the sensor along with a signal acquisition circuit enables real-time physiological signal monitoring. Various signals such as BCG, respiration, and body motion have been successfully recognized by the CPF-based smart cushion system from individuals in recumbent or seated postures. Additionally, the CPF-based piezoelectric sensor is devised into a smart wristband for pulse wave detections. These applications across multiple scenarios offer practical insights for the development of next-generation smart health monitoring devices.

EXPERIMENTAL SECTION

Fabrication Process of the Sensor

The fabrication process began with coating silver on the PVDF film. A silver-coated piezoelectric PVDF film (Shenzhen ZMK Tech Co., Ltd.) was laser-cut into strips with dimensions of 10 mm × 60 mm by using a laser engraver (VLS 2.30, Universal Laser Systems). The thickness of the PVDF film was 28 μm, and the silver layer thickness was 6 μm. Conductive double-sided copper (Cu) adhesive tapes were then attached to end surfaces to serve as external electrodes. Next, the corrugated structure and its encapsulation layer were fabricated. A piece of double-sided adhesive tape with the same size as the PVDF strip was aligned to the PVDF surface and then adhered onto a predesigned corrugated mold. Ecoflex 00-30 (Smooth-On) was prepared by mixing parts A and B in a 1:1 weight ratio. The mixture was stirred for 3 min to ensure homogeneity and then degassed in a vacuum chamber for 10 min to eliminate air bubbles. The degassed Ecoflex was poured into the mold and allowed to cure at room temperature for 5 h. After curing the upper encapsulation layer, the mold and adhesive tape were carefully removed. The partially encapsulated sensor was then placed onto a flat mold, and the above steps were repeated to encapsulate the other side. The fabrication flow is shown in Figure S1.

Sensor Characterization

The calibration system consisted of the following components: a linear displacement stage (LTS300/M), a force gauge (Mark-10), a data acquisition card (National Instruments USB-6210), and a computer. Data were recorded and visualized using NI LabVIEW. To apply a controlled load to the sensor, a force gauge was mounted on the linear displacement stage perpendicularly to the sensor surface. The sensor surface was covered with a piece of an acrylic plate with dimensions of 1.5 cm × 1 cm × 2 mm to generate a uniform pressure. The output data of the sensor were acquired with a sampling rate of 50 Hz. Since piezoelectric sensors only respond to dynamic forces, the sensitivity calibration was conducted by applying cyclic dynamic loading using computer-controlled motion of the displacement stage at a certain frequency. The experimental setup is shown in Figure S2.

The dynamic response and response/recovery times were characterized as shown in Figure S3. A signal generator was used to apply square-wave voltage excitations of varying frequencies to a piezoelectric ceramic plate (model 60-30, Shenlei Ultrasonic Materials) across its electrodes. This induced mechanical vibrations at corresponding frequencies served as the vibration source. The sensor was placed tightly on top of the vibrating piezoelectric ceramic plate. The data were recorded by the data acquisition card.

RESULTS AND DISCUSSION

Working Principle of the Sensor

Figure 1a illustrates a conceptual scenario of a smart bed cushion based on the proposed CPF sensor for contactless physiological signal monitoring. The smart cushion enables real-time tracking of cardiac and respiratory activity without requiring complex instrumentation attached to the human body. The key component of this system relies on a flexible piezoelectric sensor based on a corrugated PVDF film (Figure 1b). The schematic structure of the sensor is depicted

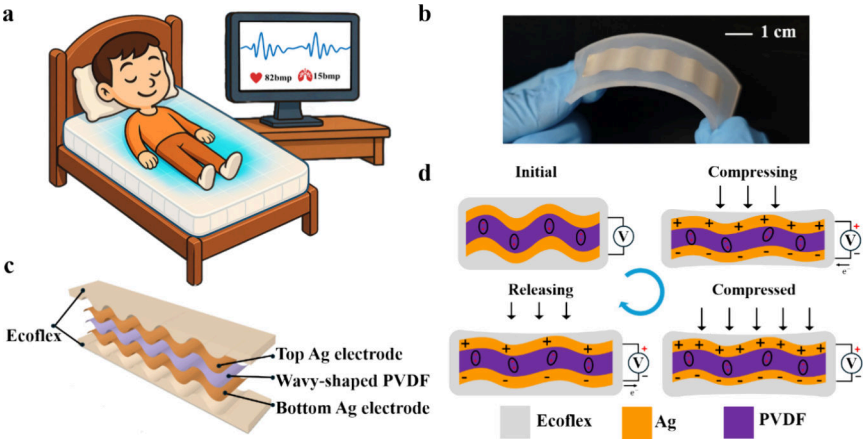


Figure 1. (a) Conceptual diagram of the smart cushion for contactless physiological signal monitoring. (b) Optical image of the corrugated PVDF sensor. (c) Schematic illustration of the corrugated PVDF sensor, including a wavy-shaped PVDF film coated with silver on both sides and an Ecoflex encapsulation layer. (d) Schematic diagram of the working principle of the corrugated PVDF sensor.

https://doi.org/10.1021/acssensors.5c04749
ACS Sens. 2026, 11, 2731−2740

Downloaded from pubs.acs.org/ascelj/article-pdf/11/3/2731/6490049/se-2025-04749j.pdf by SOOCHOW UNIV user on 13 October 2026

in Figure 1c. The sensing layer consists of a corrugated PVDF film with silver electrodes coated on top and bottom surfaces. This sensing layer is encapsulated within the soft Ecoflex elastomeric polymer.

In principle, the PVDF film converts mechanical energy into an electrical signal via the direct piezoelectric effect. The piezoelectric response of the sensor is directly proportional to the degree of deformation of the piezoelectric material. The wavy geometry can be regarded as a series of continuous semiarched structures, which are inherently sensitive to compression. As illustrated in Figure 1d, when subjected to mechanical loading, the Ecoflex layer undergoes vertical deformation, which in turn induces multidirectional coupling stress within the corrugated PVDF film. As a result, the molecular chains within PVDF deform, leading to dipole realignment and the generation of equal amounts of positive and negative charges on opposite surfaces, which is expressed externally as a potential difference. When the applied force is removed, the dipoles return to their original state.[35−37] The silver electrodes coated on the top and bottom surfaces efficiently collect these induced positive and negative charges to the external circuit. Importantly, the structural configuration of the wave shape amplifies the spatial deformation of the PVDF layer, significantly enhancing the piezoelectric output of the sensor.

Piezoelectric Responses of the Sensors with Different Wave Heights

The piezoelectric response of the sensor is closely related to the degree of deformation of the PVDF film. To investigate the influence of different wave heights on the sensor performance, both simulation analysis and experimental validation have been conducted. Four types of sensors with wave heights of 0 (flat), 1, 2, and 3 mm (the height is defined as the peak-to-valley distance of the wave) have been constructed for finite-element simulation analysis (Figure S4). Figure 2a exhibits the stress distributions of the PVDF films in the four different types of sensors under a uniform force of 7 N (or 5 kPa). In order to clearly illustrate the stress distribution in PVDF films, the Ecoflex layer is hidden. As expected, the flat (no wave) structure shows the lowest and most uniform stress distribution, with an average value of only 6.2 kPa. The stress increases with the wave height. In particular, the 1 mm-wave sensor generates an average stress of 91 kPa in PVDF, which is primarily concentrated at the peaks. The 2 mm-wave structure shows significantly increased stress with the average value of 196 kPa. The 3 mm-wave structure produces the highest stress, which is 274 kPa in average.

The four types of sensors have been also fabricated for experimental validation. The optical images are shown in Figure 2b.

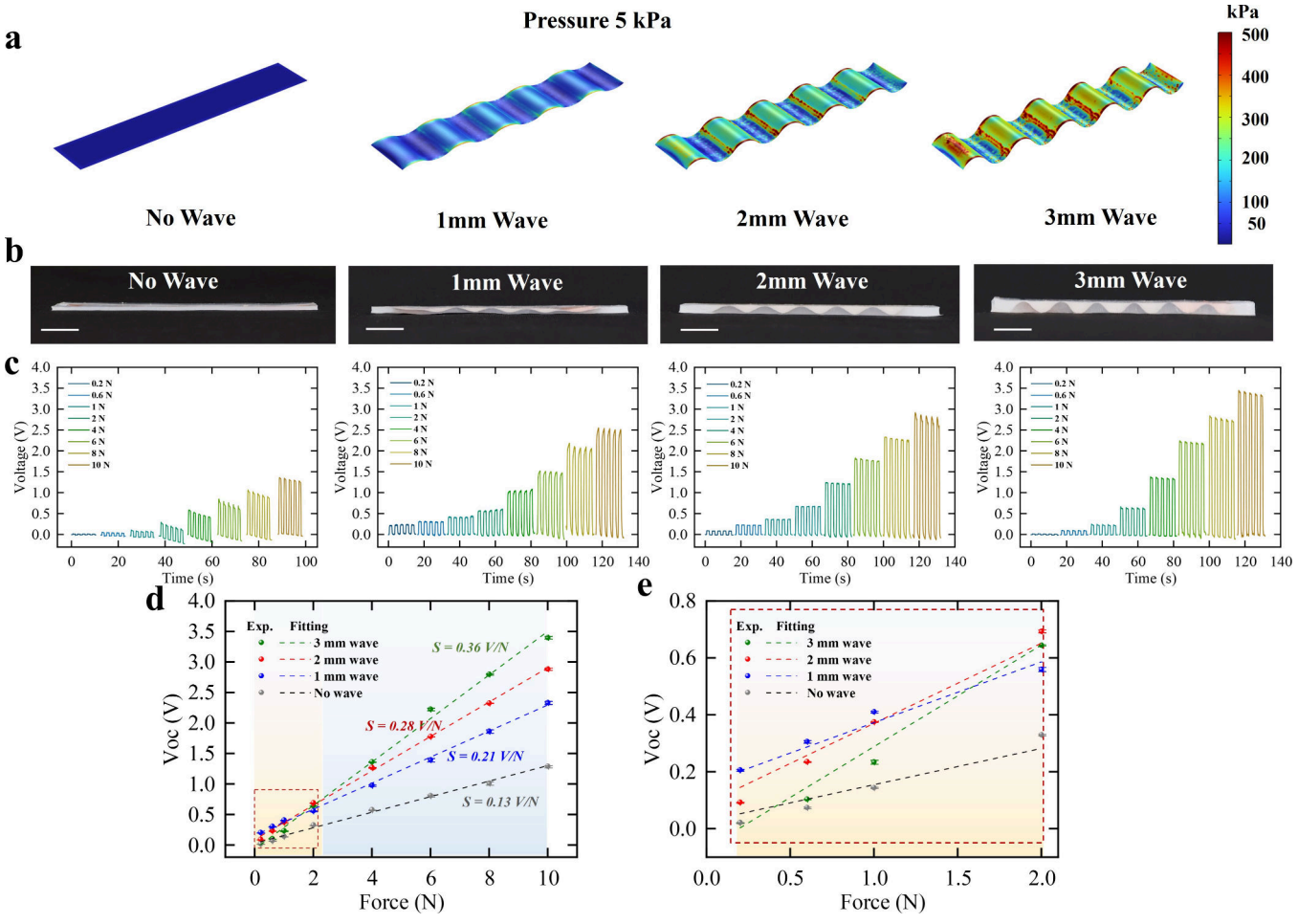


Figure 2. (a) Stress distribution of PVDF films with different wave heights when the four sensors are under a pressure of 5 kPa (or 7 N). (b) Photographs of sensors with different wave heights of 0, 1, 2, and 3 mm. Scar bar: 1 cm. (c) Output voltages under cyclic dynamic loads ranging from 0.2 to 10 N. The data from the left figure to the right figure corresponds to the sensor with wave heights of 0, 1, 2, and 3 mm. (d) Relationship between output voltage V_{oc} and the applied force derived from experimental data in (c). (e) Enlarged view of the relationship between output voltage V_{oc} and the applied force in the low force region.

Downloaded from pubs.acs.org/ascelj/article-pdf/11/3/2731/6490049/se-2025-04749j.pdf by SOOCHOW UNIV user on 13 October 2026

https://doi.org/10.1021/acssensors.5c04749
ACS Sens. 2026, 11, 2731−2740

The thickness of the encapsulated elastic layers above the wave peak and below the wave valley is fixed at 0.5 mm, making the total height of the sensor 1 mm greater than the wave height. The open-circuit voltage of sensors with different wave heights has been recorded under dynamic loading (Figure 2c). The piezoelectric output increases progressively with the applied load. The average open-circuit voltage (V_{oc}) values under varying loads (F) are used to derive the sensitivity of the sensor. Figure 2d shows the relationship between V_{oc} and F of the four sensor types, with dashed lines representing finite-element simulation results. The sensor sensitivity (S) is defined as $S = \Delta V_{oc}/\Delta F$.

As shown, all the four sensors show a linear increment in V_{oc} along with the applied force ranging from 0 to 10 N. The sensitivities of sensors with 0, 1, 2, and 3 mm wave heights are 0.13, 0.21, 0.28, and 0.36 V/N, respectively. Interestingly, in the low force region of 0−2 N in Figure 2e, the device with a 1 mm wave height shows higher voltage output, followed by that of a 2 mm-wave height sensor. This phenomenon is possibly due to the introduction of a contact-separation triboelectric voltage signal during the measurement process, resulting in the actual output voltage being a mixed signal of triboelectric voltage and piezoelectric voltage.[35] For devices with different wave heights, the equivalent thickness of their friction layer (i.e., Ecoflex in our sensor) varies. According to a previous study,[38] if the thickness of the friction layer exceeds 200 μm, further increases in thickness lead to a decrease in the triboelectric voltage output of the device. Therefore, the device with a 1 mm-wave height generates a stronger triboelectric voltage signal due to its thinner effective Ecoflex friction layer. In the low-force range where the piezoelectric effect is not yet significant, the magnitudes of the triboelectric voltage and piezoelectric voltage are comparable. At this point, the total output voltage of the 1 mm-wave height device is the highest. As the force increases, the contribution of the piezoelectric effect to the voltage becomes significantly stronger, and the total output voltage is then dominated by the piezoelectric voltage. According to simulation analysis, a higher wave height results in greater deformation and stress in PVDF under the same applied force. Thus, in the high-force range, the device with a 3 mm-wave height exhibits the highest total output voltage.

In addition, the influence of the wavelength on the sensor output has been investigated (Figure S5 in the Supporting Information). As the length of the corrugated PVDF increases from 3 to 12 cm, the output voltage decreases significantly from 4.7 to 1.6 V under the same applied force of 10 N. In practical usage, the BCG signal detection requires high device sensitivity. Meanwhile, the development of a smart cushion mat needs a compact integration with a thin device thickness. Therefore, the 2 mm-wave height offers the best trade-off between performance and structural compactness. It is selected for subsequent performance evaluation and application demonstrations.

Performance Characteristics of the Corrugated PVDF Piezoelectric Sensor

To evaluate the repeatability of the sensor under cyclic loads, a loading−unloading test has been conducted by applying a periodic force with a vibrating frequency of 10 Hz. In particular, a sine-wave signal is applied to a piezoelectric ceramic plate to act as a vibration source. The sampling rate for data acquisition is set to 100 Hz. As shown in Figure 3a, the piezoelectric response exhibits a stable periodic waveform with a peak amplitude of 0.3 V and a cycle period of 0.1 s. After about 24,000 loading cycles, no significant degradation in output signal is observed, indicating excellent repeatability and mechanical durability of the sensor. Additionally, Figure 3b exhibits the minimum resolution of the sensor. When an object with a mass of 0.098 g (38 Pa) is placed on the sensor surface, the sensor clearly distinguishes the force with a voltage increment of 4 mV.

The dynamic response reflects the range of signal frequencies that the sensor can detect. To characterize the dynamic behavior when the sensor is subjected to input signals with varying frequencies, a periodic force has been applied on the sensor. In particular, square-wave signals with a fixed amplitude of 4 V and varying frequencies are applied to a piezoelectric ceramic plate to act as a vibration source. The sampling rate for data acquisition is set to 50 Hz. As illustrated in Figure 3c, the sensor exhibits stable responses to five different frequencies from 2 to 10 Hz, confirming its ability to detect signals across a range that encompasses typical heart rate frequencies. Remarkably, the sensor is also responsive to a dynamic force with a higher frequency of 100 Hz (Figure S6).

The response and recovery times have been characterized from the time-resolved sensor output voltage. A 10 Hz square-wave signal with an amplitude of 2 V is applied to the piezoelectric ceramic plate as the vibration source, and the sampling rate of the data acquisition system is set to 10,000 Hz. Figure 3d demonstrates the rapid and consistent response to the periodic load. It is notable that the voltage did not return fully to zero. This is likely because the piezoelectric actuator did not completely separate from the sensor during its reverse vibration cycle, possibly leaving a residual force on the sensor. The rising and falling edges along with the oscillations from the piezoelectric excitation are enlarged in Figure 3e. Based on the highlighted yellow (rising edge) and blue (falling edge) regions, both the response time and recovery time are estimated to be less than 0.1 ms, indicating the excellent fast dynamic response of the CPF-based piezoelectric sensor.

Performance Comparison of Piezoelectric Pressure Sensors Based on PVDF

Table 1 compares the performance between the proposed wavy-structured PVDF flexible pressure sensor and previously reported PVDF piezoelectric sensors in the literature. Most current designs of high-performance piezoelectric sensors primarily focus on enhancing piezoelectric properties and output response by doping functional materials into the PVDF matrix.[39−43] Although such strategies demonstrate certain performance improvements under experimental conditions, they often involve complex synthesis procedures and difficulties in composition control. References 41 and 44 achieve high device sensitivities of 0.49 and 0.53 V/N, respectively, by employing a relatively complex electrostatic spinning fabrication method.

In comparison, the wavy-structured PVDF thin-film piezoelectric sensor proposed in this study not only possesses a simple fabrication process but also exhibits superior overall performance. Its sensitivity is comparable to those in the state-of-the-art techniques. Additionally, the CPF sensor exhibits a faster response time and outstanding fatigue resistance, allowing long-term and stable continuous signal acquisition in real-time physiological signal monitoring applications, thereby ensuring consistent high-quality data support in practical use.

Physiological Signal Detections Based on the Corrugated PVDF Piezoelectric Sensor

Sleep is a vital component of human health, and sleep disorders become a pressing public health concern.[45,46] Contactless sleep monitoring aims to track physiological signals such as the

Downloaded from pubs.acs.org/ascelj/article-pdf/11/3/2731/6490049/se-2025-04749j.pdf by SOOCHOW UNIV user on 13 October 2026

https://doi.org/10.1021/acssensors.5c04749
ACS Sens. 2026, 11, 2731−2740

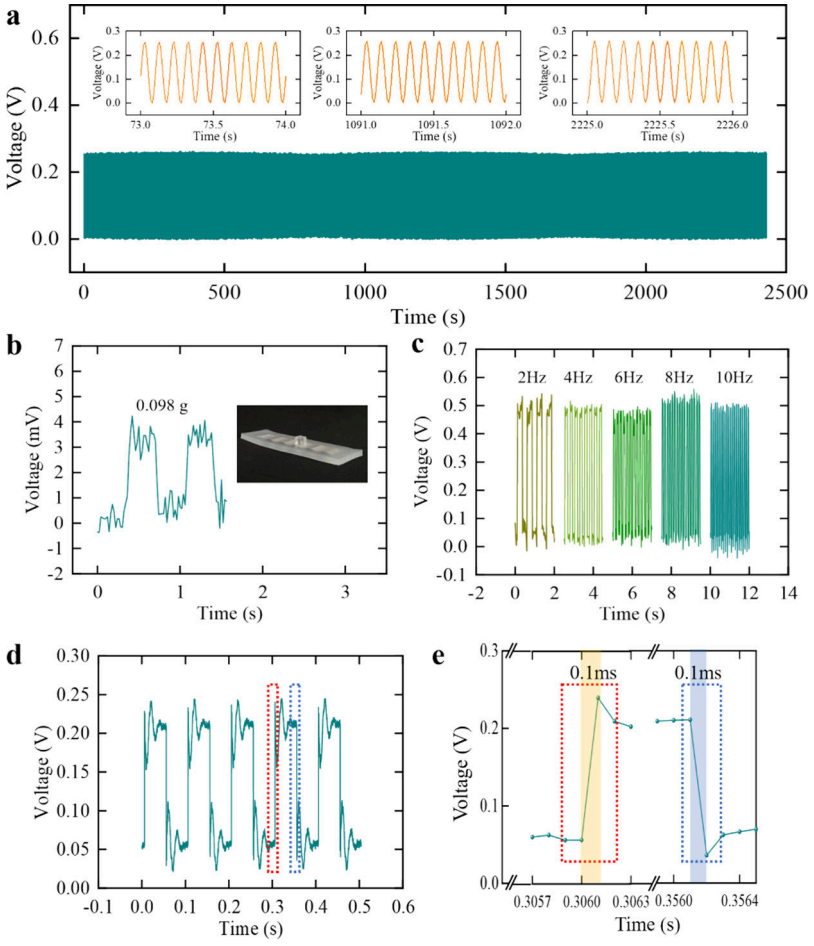


Figure 3. (a) Voltage output of the sensor under cyclic loads (about 24,000 cycles). The inset figures show the sensor voltage outputs in the period of 73, 1091, and 2225 s. (b) Voltage changes of the sensor when a tiny block is placed on its surface. (c) Piezoelectric response of the sensor under dynamic loads at different frequencies of 2, 4, 6, 8, and 10 Hz. (d) Piezoelectric response of the sensor under 10 Hz vibration force excitation. (e) Enlarged rising and falling edges of one cycle of the output voltage, showing response time and recovery time.

heart rate, respiration, and body movements. Among these, the heart rate can be inferred from BCG, which records subtle mechanical vibrations generated by cardiac activity. Such a system for BCG detection is promising for continuous, user-friendly, and cost-effective monitoring of sleep quality.[47] The corrugated PVDF piezoelectric sensor demonstrates high sensitivity to subtle physiological vibrations such as heartbeat, respiration, and body movements. Accordingly, a smart cushion system has been developed to visualize and analyze these signals in real time, as illustrated in Figure 4a. It comprises two identical cascaded stages, each consisting of a CPF sensor, a charge-to-voltage conversion module, an amplification module, and a low-pass filter

Table 1. Performance Comparison of Piezoelectric Pressure Sensors Based on PVDF

ref	materials	fabrication method	sensitivity (V N^{-1})	response time (ms)	size (cm)	duration cycles
39	PVDF/CeO_2@PDA	electrostatic spinning	0−2.3 N: 5.64 2.3−11 N: 0.38 11−23 N: 0.089	49	1.5 × 1.5	10,000
40	PVDF/BTO/NaCl	compression molding	0.083		4 × 4	12,000
41	PVDF/MXene	electrostatic spinning	0.49		1.1 × 1.1	14,000
42	MXene/PVDF-TrFE	solution casting	0.088	40	2 × 2	10,000
43	PVDF/ZnO	electrostatic spinning	0.013	8	1 × 1	2000
44	PVDF	electrostatic spinning/knitting	0.53			3350
this work	PVDF	3D molding	0.36	<0.1	7 × 2	24,00

https://doi.org/10.1021/acssensors.5c04749
ACS Sens. 2026, 11, 2731−2740

Downloaded from pubs.acs.org/ascelj/article-pdf/11/3/2731/6490049/se-2025-04749j.pdf by SOOCHOW UNIV user on 13 October 2026

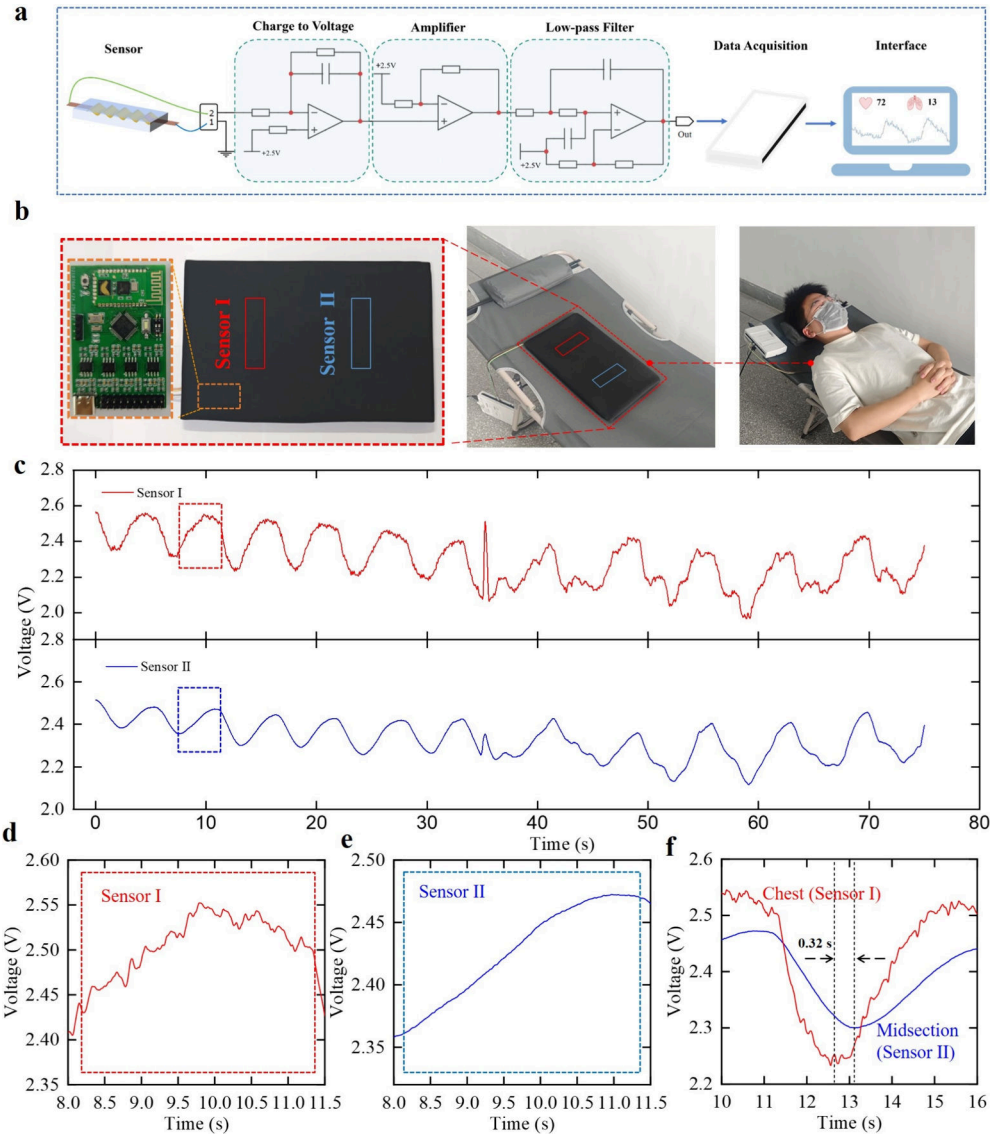


Figure 4. (a) Block diagram of the physiological signal acquisition system. (b) Photograph of the smart cushion embedded with the sensor and the acquisition circuit and photograph of a volunteer lying on the mat for BCG and respiration signal measurement. (c) Dual-channel signals continuously recorded for 75 s from a 22-year-old male volunteer. (d) Enlarged signal recorded by sensor I (thoracic region). (e) Enlarged signal recorded by sensor II (abdominal region). (f) Phase difference between the two waveforms recorded by sensor I and sensor II.

module. One terminal of each sensor is connected to the input of its corresponding cascaded stage, while the other terminal is grounded. The output signals from the cascaded stages are fed into the input ports of a data acquisition card and are ultimately displayed in real time on a computer terminal. The two flexible CPF piezoelectric sensors with dimensions of 70 mm × 20 mm × 3 mm and a separation distance of 20 cm are embedded in a mat shown in Figure 4b. A 22-year-old male volunteer lies on the smart mat for real-time monitoring of sleep-related physiological signals. The voltage outputs of the two sensors have been recorded for 75 s, to mimic the continuous sleep monitoring condition. As shown in Figure 4c, distinct waveform patterns have been observed from two sensor channels. Sensor I, which is placed at the thoracic region, captures richer physiological information than sensor II. For example, sensor I shows respiratory waveforms superimposed with clear BCG signals (enlarged in Figure 4d). In contrast, sensor II, which is located near the abdomen/back, records only respiratory waveforms at the same time period (enlarged Figure 4e). In respiratory physiology, thoracic and abdominal breathing represents a biomechanically coupled system. Since the volunteer predominantly exhibited thoracic breathing, thoracic motion preceded abdominal motion and exhibited a larger amplitude. As shown in Figure 4f, the respiratory waveform from sensor II lags behind that of sensor I by approximately 0.32 s. The amplitudes of the respiratory waveform are approximately 0.25 V for sensor I and 0.14 V for sensor II.

Analysis on the Heart Rate and Respiratory Signals

The heart rate and respiratory rate are two critical physiological indicators and serve as essential parameters in sleep monitoring.[48] To further analyze cardiac and respiratory information, sensor I is selected in this section. Continuous 110 s signals have been recorded from a 24-year-old female volunteer when she lies on the smart cushion. Figure 5a shows different

Downloaded from pubs.acs.org/ascelj/article-pdf/11/3/2731/6490049/se-2025-04749j.pdf by SOOCHOW UNIV user on 13 October 2026

https://doi.org/10.1021/acssensors.5c04749
ACS Sens. 2026, 11, 2731−2740

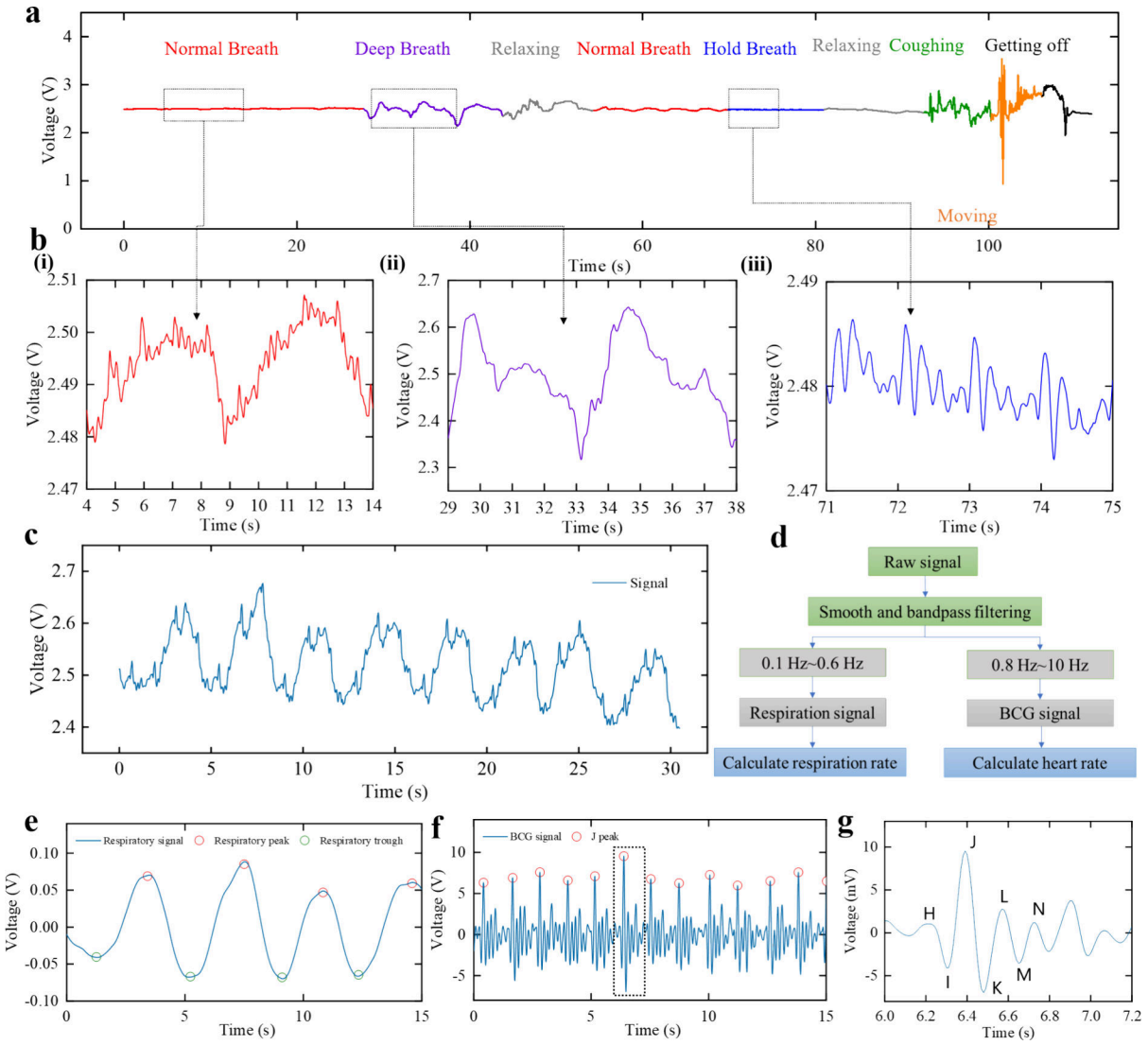


Figure 5. (a) Representative waveforms under different physiological states imitated by the volunteer in the sleep cycle. (b) Enlarged views of signal waveforms in (i) normal breathing, (ii) deep breathing, and (iii) breath-holding states. (c) Raw signal during normal breathing. (d) Flowchart of the signal processing algorithm for extracting respiratory and BCG waveforms. (e) Extracted respiratory waveform from the raw data in (c). (f) Extracted BCG waveform from the raw data in (c). (g) Single cycle of the BCG waveform, showing characteristic H−N points.

stages including normal breathing, deep breathing, relaxation (the process of restoring normal respiration), breath-holding, coughing, body movements, and leaving the bed. Normal breathing, deep breathing, and breath-holding stages exhibit distinct waveform characteristics. The normal breathing brings a respiratory waveform with a frequency of 0.2 Hz and an amplitude of 22 mV (Figure 5b(i)). In deep breathing, the breath frequency is the same as 0.2 Hz, while the amplitude increases to 310 mV (Figure 5b(ii)). Both signals superimpose with clear BCG signals. In contrast, during breath-holding, only BCG signals are observed and there is no obvious respiration signal (Figure 5b(iii)). In the clinic, deep breathing and breath-holding may reflect physiological regulation or potential pathological states, such as sleep apnea syndrome or other respiratory disorders.[49] The smart cushion can provide a convenient solution for sleep state monitoring.

As illustrated in Figure 5c, the raw signal acquired through the sensor contains a low-frequency, high-amplitude respiratory waveform, along with a superimposed high-frequency, low-amplitude BCG waveform. In addition, nonphysiological high-frequency noise may also be present in the raw signal. To extract respiratory and heart rate information, a combination of a smoothing filter and a Butterworth band-pass filter is applied to preprocess the raw data (Figure 5d). A dynamic thresholding algorithm is used to detect respiratory peaks and troughs, allowing for calculation of the respiration rate based on peak intervals. Similarly, the *J*-peaks in the BCG waveform are identified to compute the heart rate via *J*−*J* interval analysis. Figure 5e displays the extracted respiratory signal with annotated peaks and troughs, yielding a respiration rate of 16.03 bpm. Figure 5f shows a clean BCG waveform after filtering, with identified *J*-peaks used to calculate an average heart rate of 50.72 bpm. A BCG cycle is enlarged in Figure 5g, where the sensor successfully captures key morphological features, demonstrating its capability for accurate BCG monitoring.

Pulse Waveform Detection at Other Body Locations

The CPF piezoelectric sensor is capable of capturing pulse waveforms at various body locations, such as the fingertip, radial artery, and femoral artery, to facilitate heart rate calculation. As

Downloaded from pubs.acs.org/ascelj/article-pdf/11/3/2731/6490049/se-2025-04749j.pdf by SOOCHOW UNIV user on 13 October 2026

https://doi.org/10.1021/acssensors.5c04749
ACS Sens. 2026, 11, 2731−2740

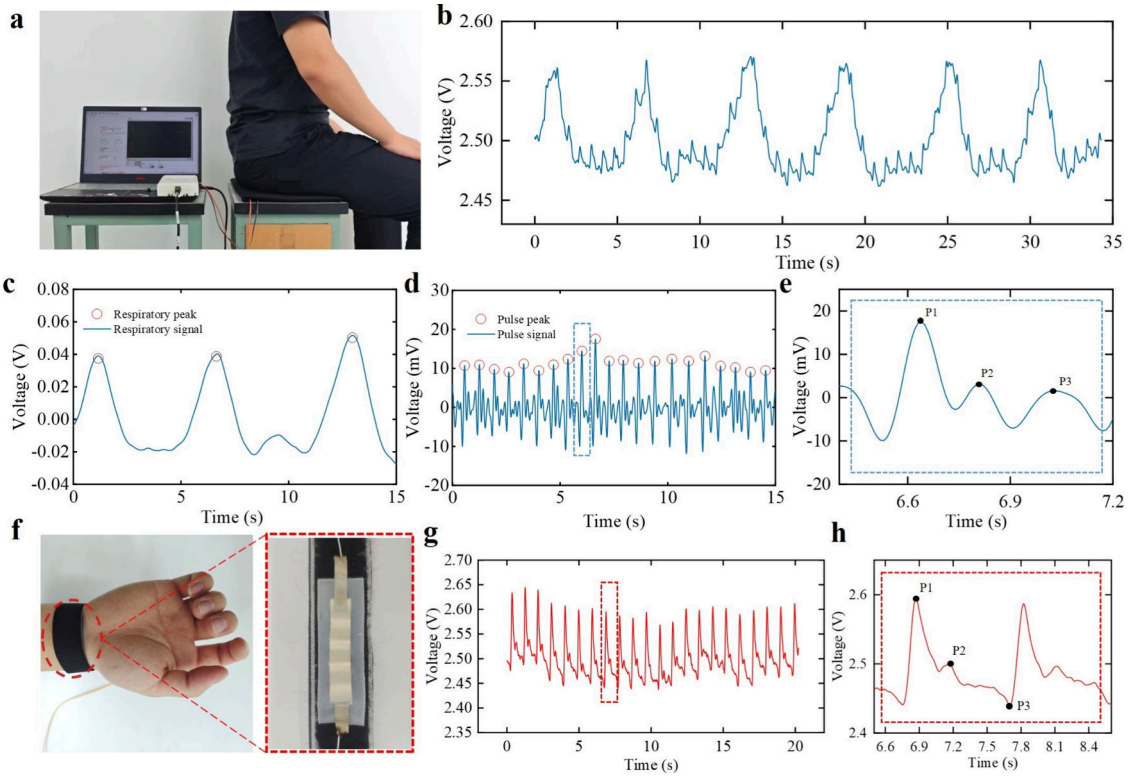


Figure 6. (a) Illustration of the sedentary monitoring scenario employing the smart cushion. (b) Raw signal acquired by the sensor when a 25-year-old male volunteer sat on the cushion. (c) Respiratory signal extracted from the raw signal in (b). (d) Femoral artery pulse signal extracted from the raw signal in (b). (e) Detailed view of a single cycle of the femoral pulse waveform, annotated with characteristic points P1, P2, and P3. (f) Photograph of a wristband integrated with the CPF-based sensor, designed for pulse monitoring at the radial artery. (g) Radial artery pulse waveform recorded from a 25-year-old male subject. (h) Single pulse cycle from the radial waveform, indicating the characteristic points P1, P2, and P3.

shown in Figure 6a, the smart cushion is placed on a seat for contactless monitoring of the femoral artery waveform while a 25-year-old male volunteer is seated. Figure 6b presents the raw signal recorded from the volunteer seated on the cushion for 35 s. Similarly, the acquired signal contains both respiratory and pulse waveform components. Through signal processing, the respiratory waveform (Figure 6c) and pulse waveform (Figure 6d) have been successfully extracted, allowing for the calculation of the respiratory rate and heart rate as 10.83 and 79.84 bpm, respectively. Figure 6e displays a cycle of the extracted pulse waveform, showing the three characteristic peaks of P1, P2, and P3. This demonstration presents a promising approach for prolonged sitting alteration, which may reduce health risks from chronic cerebrovascular and respiratory diseases. [50−52] In addition, the sensor is wrapped around the wrist of a 25-year-old male volunteer (Figure 6f), and a time-resolved radial artery pulse waveform is acquired (Figure 6g). A representative waveform of a single cardiac cycle is displayed in Figure 6h, clearly showing three characteristic points of P1, P2, and P3. Overall, the corrugated PVDF-based piezoelectric sensor enables heart rate estimation in a wide range of scenarios and is promising in assisting the early diagnosis of potential cardiovascular conditions.

CONCLUSIONS

In this study, a flexible piezoelectric sensor based on a corrugated PVDF film has been designed and fabricated. The piezoelectric PVDF sensing layer is engineered into a corrugated configuration, which enhances spatial deformability and enables the sensor to sensitively detect external force distributions and variations with high resolution. The performance evaluation of the sensor demonstrates a high sensitivity of up to 0.36 V/N and a minimum detectable force of 98 mg. Cyclic loading tests confirmed the excellent stability and repeatability in practical applications. Furthermore, both the response time and recovery time are less than 0.1 ms, indicating a rapid response capability well-suited for capturing subtle and fast physiological movements. The sensor was successfully integrated into a soft bed cushion for physiological signal monitoring. The sensor is capable of detecting pulse signals from multiple anatomical locations. The results highlight the promising potential of the sensor in healthcare-related applications, such as clinical tracking, personal health monitoring, and early disease detection.

ASSOCIATED CONTENT

Data Availability

The data that support the findings of this study are available from the corresponding author upon reasonable request.

Supporting Information

The Supporting Information is available free of charge at https://pubs.acs.org/doi/10.1021/acssensors.5c04749.

Fabrication process of the sensor (Figure S1); sensor characterization (Figures S2 and S3); numerical model for finite-element simulation (Figure S4); investigation on the effect of the wavelength on the sensing performance

https://doi.org/10.1021/acssensors.5c04749
ACS Sens. 2026, 11, 2731−2740

Downloaded from pubs.acs.org/ascelj/article-pdf/11/3/2731/6490049/se-2025-04749j.pdf by SOOCHOW UNIV user on 13 October 2026

(Figure S5); dynamic response of the sensor under a vibrating force at 100 Hz (Figure S6) (DOCX)

AUTHOR INFORMATION

Corresponding Author

Baoqing Nie − *School of Electronic and Information Engineering, Soochow University, Suzhou, Jiangsu 215006, China;* orcid.org/0000-0003-4631-0728; Email: qixinbq@suda.edu.cn

Authors

Ziqiong Cao − *School of Electronic and Information Engineering, Soochow University, Suzhou, Jiangsu 215006, China*

Donglin Wu − *School of Electronic and Information Engineering, Soochow University, Suzhou, Jiangsu 215006, China*

Yaojun Yuan − *School of Electronic and Information Engineering, Soochow University, Suzhou, Jiangsu 215006, China*

Rui Hu − *School of Electronic and Information Engineering, Soochow University, Suzhou, Jiangsu 215006, China*

Jiaqi Zhang − *School of Electronic and Information Engineering, Soochow University, Suzhou, Jiangsu 215006, China*

Enting Gao − *School of Electronic and Information Engineering, Suzhou University of Science and Technology, Suzhou, Jiangsu 215009, China*

Xinjian Chen − *School of Electronic and Information Engineering, Soochow University, Suzhou, Jiangsu 215006, China*

Xuemei Lu − *Jiangsu Key Laboratory of Biophotonics, Suzhou City University, Suzhou, Jiangsu 215104, China;* orcid.org/0009-0005-7590-9475

Xiaoyu Tang − *Academy of Pharmacy, Xi'an Jiaotong-Liverpool University, Suzhou, Jiangsu 215123, China*

Complete contact information is available at: https://pubs.acs.org/doi/10.1021/acssensors.5c04749

Notes

The authors declare no conflicts of interest.

ACKNOWLEDGMENTS

This work was supported by the National Natural Science Foundation of China (Nos. 62471326 and 22203059), Jiangsu Key Laboratory of Biophotonics Open Projects Fund (Project Nos. 2025BPT003 and 2025BPT004), Qing Lan Project, and Research Development Fund at Xi'an Jiaotong-Liverpool University (Grant No. RDF2401022).

REFERENCES

(1) Sim, D.; Brothers, M. C.; Slocik, J. M.; Islam, A. E.; Maruyama, B.; Grigsby, C. C.; Naik, R. R.; Kim, S. S. Biomarkers and detection platforms for human health and performance monitoring: A review. *Adv. Sci.* **2022**, *9* (7), No. 2104426.

(2) Choi, J. S.; Lee, H. J.; Rajaraman, S.; Kim, D.-H. Recent advances in three-dimensional microelectrode array technologies for in vitro and in vivo cardiac and neuronal interfaces. *Biosens. Bioelectron.* **2021**, *171*, No. 112687.

(3) Pang, Q.; Hu, H.; Zhang, H.; Qiao, B.; Ma, L. Temperature-responsive ionic conductive hydrogel for strain and temperature sensors. *ACS Appl. Mater. Interfaces* **2022**, *14* (23), 26536.

(4) Rastegar, S.; GholamHosseini, H.; Lowe, A. Non-invasive continuous blood pressure monitoring systems: Current and proposed technology issues and challenges. *Phys. Eng. Sci. Med.* **2020**, *43* (1), 11–28.

(5) Zhang, T.; Liu, N.; Xu, J.; Liu, Z.; Zhou, Y.; Yang, Y.; Li, S.; Huang, Y.; Jiang, S. Flexible electronics for cardiovascular healthcare monitoring. *Innovation* **2023**, *4* (5), No. 100485.

(6) Sun, J.; Xiu, K.; Wang, Z.; Hu, N.; Zhao, L.; Zhu, H.; Kong, F.; Xiao, J.; Cheng, L.; Bi, X. Multifunctional wearable humidity and pressure sensors based on biocompatible graphene/bacterial cellulose bioaerogel for wireless monitoring and early warning of sleep apnea syndrome. *Nano Energy* **2023**, *108*, No. 108215.

(7) Hannun, A. Y.; Rajpurkar, P.; Haghpanahi, M.; Tison, G. H.; Bourn, C.; Turakhia, M. P.; Ng, A. Y. Cardiologist-level arrhythmia detection and classification in ambulatory electrocardiograms using a deep neural network. *Nat. Med.* **2019**, *25* (1), 65–69.

(8) Al-Khalidi, F. Q.; Saatchi, R.; Burke, D.; Elphick, H.; Tan, S. Respiration rate monitoring methods: A review. *Pediatr. Pulmonol.* **2011**, *46* (6), 523–529.

(9) Lubitz, S. A.; Faranesh, A. Z.; Selvaggi, C.; Atlas, S. J.; McManus, D. D.; Singer, D. E.; Pagoto, S.; McConnell, M. V.; Pantelopoulos, A.; Foulkes, A. S. Detection of atrial fibrillation in a large population using wearable devices: The fitbit heart study. *Circulation* **2022**, *146* (19), 1415–1424.

(10) Zhou, Z.; Padgett, S.; Cai, Z.; Conta, G.; Wu, Y.; He, Q.; Zhang, S.; Sun, C.; Liu, J.; Fan, E.; et al. Single-layered ultra-soft washable smart textiles for all-around ballistocardiograph, respiration, and posture monitoring during sleep. *Biosens. Bioelectron.* **2020**, *155*, No. 112064.

(11) Zhou, Z.; Jin, Y.; Fu, J.; Si, S.; Liu, M.; Hu, Y.; Gan, J.; Deng, Y.; Li, R.; Yang, J. Smart wireless flexible sensing system for unconstrained monitoring of ballistocardiogram and respiration. *npj Flexible Electron.* **2025**, *9* (1), 15.

(12) Si, S.; Sun, C.; Wang, H.; Wu, H.; Chen, L.; Xia, Y.; Qin, J.; Wu, Y.; Yang, J. Unconstrained blood pressure monitoring based on a neural network–assisted multistage pressure textile sensor. *Nano Energy* **2023**, *115*, No. 108730.

(13) Clausen, T.; Jura, T.; Jähne-Raden, N.; Wolf, M. C.; Wolf, L.; Kulau, U. A precise, parallel and scalable measurement system for ballistocardiographic research. *Smart Health* **2021**, *19*, No. 100169.

(14) Czapanskiy, M. F.; Ponganis, P. J.; Fahlbusch, J. A.; Schmitt, T. l.; Goldbogen, J. A. An accelerometer-derived ballistocardiogram method for detecting heart rate in free-ranging marine mammals. *J. Exp. Biol.* **2022**, *225* (10), No. 243872.

(15) Chen, S.; Luo, H.; Lyu, W.; Yu, J.; Qin, J.; Yu, C. Compressed sensing framework for bcg signals based on the optical fiber sensor. *Opt. Express* **2023**, *31* (18), 29606–29618.

(16) Singh, J. Development trends in the sensor technology: A new bcg matrix analysis as a potential tool of technology selection for a sensor suite. *IEEE Sens. J.* **2004**, *4*, 664–669.

(17) Gu, X.; Zhang, L.; Xiao, Y.; Zhang, H.; Hong, H.; Zhu, X. Non-contact fatigue driving detection using cw doppler radar. In *2018 IEEE MTT-S International Wireless Symposium* (*IWS*); IEEE: Chengdu, China, 2018.

(18) Tran, V. P.; Al-Jumaily, A. A.; Islam, S. M. Doppler radar-based non-contact health monitoring for obstructive sleep apnea diagnosis: A comprehensive review. *Big Data Cognit. Comput.* **2019**, *3* (1), 3.

(19) Li, Y. X.; Huang, J. L.; Yao, X. Y.; Mu, S. Q.; Zong, S. X.; Shen, Y. F. A ballistocardiogram dataset with reference sensor signals in long-term natural sleep environments. *Sci. Data* **2024**, *11* (1), 1091.

(20) Kumaki, D.; Motoshima, Y.; Higuchi, F.; Sato, K.; Sekine, T.; Tokito, S. Unobstructive heartbeat monitoring of sleeping infants and young children using sheet-type pvdf sensors. *Sensors* **2023**, *23* (22), 9252.

(21) Pauli, M.; Göttel, B.; Scherr, S.; Bhutani, A.; Ayhan, S.; Winkler, W.; Zwick, T. Miniaturized millimeter-wave radar sensor for high-accuracy applications. *IEEE Trans. Microwave Theory Tech.* **2017**, *65* (5), 1707–1715.

(22) Butt, M. A.; Voronkov, G. S.; Grakhova, E. P.; Kutluyarov, R. V.; Kazanskiy, N. L.; Khonina, S. N. Environmental monitoring: A comprehensive review on optical waveguide and fiber-based sensors. *Biosensors* **2022**, *12* (11), 1038.

Downloaded from pubs.acs.org/ascelj/article-pdf/11/3/2731/6490049/se-2025-04749j.pdf by SOOCHOW UNIV user on 13 October 2026

(23) Mao, A.; Lu, W.; Jia, Y.; Wang, R.; Sun, J. Flexible piezoelectric devices and their wearable applications. *J. Inorg. Mater.* **2023**, *38* (7), 717–730.
(24) Yi, Z.; Liu, Z.; Li, W.; Ruan, T.; Chen, X.; Liu, J.; Yang, B.; Zhang, W. Piezoelectric dynamics of arterial pulse for wearable continuous blood pressure monitoring. *Adv. Mater.* **2022**, *34* (16), No. 2110291.
(25) Habib, M.; Lantgios, I.; Hornbostel, K. A review of ceramic, polymer and composite piezoelectric materials. *J. Phys. D: Appl. Phys.* **2022**, *55* (42), 423002.
(26) Ghadarah, N.; Ayre, D. A review on acoustic emission testing for structural health monitoring of polymer-based composites. *Sensors* **2023**, *23* (15), 6945.
(27) Hou, T.; Tong, J.; wang, Y.; Cui, M.; Yan, Y.; Xin, Y. An overpressure monitoring system based on pvdf integrated electronic sensor with enhanced noise attenuation capability. *Measurement* **2024**, *228*, No. 114297.
(28) Hari, M. A.; Karumuthil, S. C.; Varghese, S.; Rajan, L. Performance enhancement of flexible and self-powered pvdf-zno based tactile sensors. *IEEE Sens. J.* **2022**, *22* (10), 9336–9343.
(29) Qiu, X.; Bian, Y.; Mei, X.; Luo, X.; Hu, Z.; Xuan, F.; Xiang, Y.; Zhu, G. Fully transparent flexible piezoelectric sensing materials based on electrospun pvdf and their device applications. *Adv. Mater. Technol.* **2024**, *9* (5), No. 2301494.
(30) He, W.; Dai, Z.; Zou, K.; Li, X.; Hao, S.; Wang, H. Flexible piezoelectric pvdf nanofiber film sensor by blow spinning. *Sci. China Technol. Sci.* **2023**, *66* (3), 863–868.
(31) Peng, R.; Zhang, B.; Dong, G.; Wang, Y.; Yang, G.; Zhang, J.; Peng, B.; Zhao, Y.; Liu, M. Enhanced piezoelectric energy harvester by employing freestanding single-crystal batio3 films in pvdf-trfe based composites. *Adv. Funct. Mater.* **2024**, *34* (27), No. 2316519.
(32) Kim, Y.; Lee, J.; Hong, H.; Park, S.; Ryu, W. Self-powered wearable micropyramid piezoelectric film sensor for real-time monitoring of blood pressure. *Adv. Eng. Mater.* **2023**, *25* (2), No. 2200873.
(33) Huang, A.; Zhu, Y.; Peng, S.; Tan, B.; Peng, X. Improved energy harvesting ability of single-layer binary fiber nanocomposite membrane for multifunctional wearable hybrid piezoelectric and triboelectric nanogenerator and self-powered sensors. *ACS Nano* **2024**, *18* (1), 691–702.
(34) Zhang, Y.; Liu, C.; Jia, B.; Ma, D.; Tian, X.; Cui, Y.; Deng, Y. Kirigami-inspired, three-dimensional piezoelectric pressure sensors assembled by compressive buckling. *npj Flexible Electron.* **2024**, *8* (1), 23.
(35) Chen, C.; Zhao, S.; Pan, C.; Zi, Y.; Wang, F.; Yang, C.; Wang, Z. L. A method for quantitatively separating the piezoelectric component from the as-received "piezoelectric" signal . *Nat. Commun.* **2022**, *13* (1), 1391.
(36) Yu, D.; Zheng, Z.; Liu, J.; Xiao, H.; Huangfu, G.; Guo, Y. Superflexible and lead-free piezoelectric nanogenerator as a highly sensitive self-powered sensor for human motion monitoring. *Nano-Micro Lett.* **2021**, *13* (1), 117.
(37) Qi, F.; Xu, L.; He, Y.; Yan, H.; Liu, H. Pvdf-based flexible piezoelectric tactile sensors: Review. *Cryst. Res. Technol.* **2023**, *58* (10), No. 2300119.
(38) Lee, D.; Gu, J.; Oh, J.; Kim, K. Synergistic effects of porous ferroelectric friction layer and intermediate layers for remarkable performance enhancement of triboelectric nanogenerator. *Chem. Eng. J.* **2025**, *506*, No. 160057.
(39) Huang, S.; Zhao, X.; Hao, C.; Ma, Z.; Wang, H.; Zhang, A.; Zhang, W.; Li, L.; Zhang, W. Multifunctional pvdf/ceo$_2$@pda nanofiber textiles with piezoelectric and piezo-phototronic properties for self-powered piezoelectric sensor and photodetector. *Chem. Eng. J.* **2024**, *482*, No. 148950.
(40) Huang, Z.; Li, L.; Huang, Y.; Rao, W.; Jiang, H.; Wang, J.; Zhang, H.; He, H.; Qu, J. Self-poled piezoelectric polymer composites via melt-state energy implantation. *Nat. Commun.* **2024**, *15* (1), 819.
(41) Wang, X.; Lu, Y.; Jiang, J.; Lv, C.; Fu, H.; Xie, M. A flexible piezoelectric pvdf/mxene pressure sensor for roughness discrimination. *IEEE Sens. J.* **2024**, *24* (5), 7176–7184.
(42) Wang, Z.; Arachchi, V. W.; Alahakoon, C.; Sayem, S. H. A flexible dual-mode piezoelectric–piezoresistive sensor based on mxene/pvdf-trfe hybrid film. *IEEE Sens. J.* **2025**, *25* (12), 21141–21150.
(43) Shao, X.; Chen, Z.; Yu, J.; Lu, F.; Chen, S.; Xu, J.; Yao, Y.; Liu, B.; Yang, P.; Jiang, Q.; Hu, B. Ultralow-cost piezoelectric sensor constructed by thermal compression bonding for long-term biomechanical signal monitoring in chronic mental disorders. *Nanoscale* **2024**, *16* (6), 2974–2982.
(44) Wan, X.; Shen, Y.; Luo, T.; Xu, M.; Cong, H.; Chen, C.; Jiang, G.; He, H. All-textile piezoelectric nanogenerator based on 3d knitted fabric electrode for wearable applications. *ACS Sens.* **2024**, *9* (6), 2989–2998.
(45) Rangaraj, V. R.; Knutson, K. L. Association between sleep deficiency and cardiometabolic disease: Implications for health disparities. *Sleep Med.* **2016**, *18*, 19–35.
(46) Irwin, M. R. Why sleep is important for health: A psychoneuroimmunology perspective. *Annu. Rev. Psychol.* **2015**, *66* (1), 143–172.
(47) Zalar, P.; Burghoorn, M. M. A.; Fijn, J. A.; Rikken, L. F. A.; Rensing, P. A.; van den Brand, J.; Leeuw, D. M.; Smits, E. C. P. Large area ballistocardiography enabled by printed piezoelectric sensor arrays on elastomeric substrates. *Adv. Mater. Technol.* **2024**, *9* (17), No. 2400228.
(48) Stein, P. K.; Pu, Y. Heart rate variability, sleep and sleep disorders. *Sleep Med. Rev.* **2012**, *16* (1), 47–66.
(49) Zhu, K.; Li, M.; Akbarian, S.; Hafezi, M.; Yadollahi, A.; Taati, B. Vision-based heart and respiratory rate monitoring during sleep – a validation study for the population at risk of sleep apnea. *IEEE J. Transl. Eng. Health Med.* **2019**, *7*, 1–8.
(50) Odesola, D. F.; Kulon, J.; Verghese, S.; Partlow, A.; Gibson, C. Smart sensing chairs for sitting posture detection, classification, and monitoring: A comprehensive review. *Sensors* **2024**, *24* (9), 2940.
(51) Li, S.; Lear, S. A.; Rangarajan, S.; Hu, B.; Yin, L.; Bangdiwala, S. I.; Alhabib, K. F.; Rosengren, A.; Gupta, R.; Mony, P. K.; et al. Association of sitting time with mortality and cardiovascular events in high-income, middle-income, and low-income countries. *JAMA Cardiol.* **2022**, *8* (7), 796–807.
(52) Ma, X.; Qi, Y.; Niu, Y.; Zhang, Q.; Xiang, X.; Zhang, K.; He, P.; Dai, Y.; Niu, W.; Zhang, X. Highly sensitive, ultra-reliable flexible piezoelectret sensor for non-contact sitting motion tracking and physiological signal monitoring. *Nano Energy* **2023**, *111*, No. 108424.

Downloaded from pubs.acs.org/ascelj/article-pdf/11/3/2731/6490049/se-2025-04749j.pdf by SOOCHOW UNIV user on 13 October 2026

https://doi.org/10.1021/acssensors.5c04749
ACS Sens. 2026, 11, 2731–2740